Identifying global seismic anisotropy patterns by correlating shear-wave splitting and surface wave data

Andreas Wüstefeld, Götz Bokelmann, Guilhem Barruol, Jean-Paul Montagner

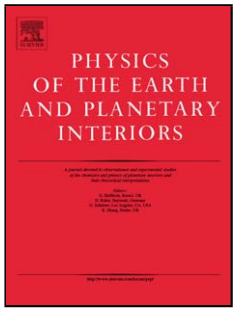

Title: Identifying global seismic anisotropy patterns by correlating shear-wave splitting and surface wave data

Authors: Andreas Wüstefeld, Götz Bokelmann, Guilhem Barruol, Jean-Paul Montagner

PII: S0031-9201(09)00126-5
DOI: doi:10.1016/j.pepi.2009.05.006
Reference: PEPI 5173

To appear in: *Physics of the Earth and Planetary Interiors*

Received date: 2-12-2008
Revised date: 8-5-2009
Accepted date: 12-5-2009

Please cite this article as: Wüstefeld, A., Bokelmann, G., Barruol, G., Montagner, J.-P., Identifying global seismic anisotropy patterns by correlating shear-wave splitting and surface wave data, *Physics of the Earth and Planetary Interiors* (2008), doi:10.1016/j.pepi.2009.05.006

Identifying global seismic anisotropy patterns by correlating shear-wave splitting and surface wave data

Andreas Wüstefeld[a,*)], Götz Bokelmann[a)], Guilhem Barruol[a)], Jean-Paul Montagner[b)]

a) Université Montpellier II, CNRS, Géosciences Montpellier, F-34095 Montpellier cedex 5, France. fax: (33) 4 67 14 36 03,

b) Institut de Physique du Globe de Paris, 4 place Jussieu, Case 89, 75005 Paris, France.

*) now at Department of Earth Sciences, University of Bristol, BS8 1RJ, United Kingdom

Abstract

We compare a global compilation of shear-wave splitting measurements with azimuthal seismic anisotropy parameters inferred from surface wave tomography. The currently available splitting dataset is taken from a novel comprehensive collection of available publications that is updated interactively online. The comparison between the two types of data is made by calculating predicted splitting parameters from the anisotropic tomography model. Comparing these predicted splitting parameters with the observed ones, we find a considerable correlation between the two datasets at global scale. This result is noteworthy, since such correlation did not seem to exist in previous studies. The spatial resolution associated with the two types of methods is rather different. While surface waves have good vertical resolution and poor lateral resolution of several hundreds of kilometers, SKS splitting measurements have good lateral, but poor vertical resolution. The correlation can be understood in light of recent propositions that anisotropy seen by SKS splitting constrains mostly the upper mantle, and therefore a similar depth region as surface waves. The correlation also confirms the generally good quality of the shear-wave measurements, as well as that of the anisotropic tomography model.

1. Introduction

Seismic waves are arguably the most powerful geophysical tools to investigate the Earth's deep interior. Anisotropy is one of the many material properties that affect seismic wave propagation. It manifests itself as a dependence of wave speed on direction. Such anisotropy can be caused by

structural variability, e.g. thin layers of alternating elastic properties (Backus, 1962) or fluid-filled cracks (Crampin, 1984; Kendall et al., 2006). A second origin which is widely accepted to dominate at mantle depths is the preferred orientation of anisotropic minerals by strain (e.g., Nicolas and Christensen, 1987). Olivine plays a major role in the anisotropy of the Earth's mantle because it represents the primary constituent of the upper mantle and is more anisotropic than the other minerals. At upper mantle conditions olivine deforms by dislocation-creep (Nicolas and Christensen, 1987), and therefore aligns its main crystallographic axes with respect to structural directions (lineation, pole of the foliation), therefore producing a large-scale anisotropy detectable by seismic waves that is correlated with the geometry of strain in the upper mantle. Identifying the orientation of seismic anisotropy and its strength can thus help to constrain deformation at depth. Comparing seismic anisotropy with other observables such as gravitation and topography (Simons and van der Hilst, 2003) or the magnetic anomalies (Bokelmann and Wüstefeld, 2009; Wüstefeld et al., 2009) is helpful for understanding tectonic processes acting within the Earth, both, ancient ones recorded within the lithosphere, and more recent ones in the asthenosphere.

Hess (1964) was the first to measure azimuthal anisotropy from Pn travel-time variations beneath the northern Pacific and to interpret these variations in terms of mantle flow induced by sea-floor spreading. Since these pioneering works, a variety of techniques have been proposed for detecting seismic anisotropy. These include relative P-wave delay times (e.g., Babuska et al., 1984; Bokelmann, 2002), P-wave polarization (Bokelmann, 1995; Schulte-Pelkum et al., 2001; 2003; Fontaine et al., 2009), shear-wave splitting (for references see below) and radial and azimuthal anisotropic surface-wave tomography (e.g., Montagner, 1986, Nishimura and Forsyth, 1988; Montagner and Tanimoto, 1991).

The most direct evidence of seismic anisotropy is the splitting of shear-waves. Anisotropic media are indeed birefringent, splitting the incoming shear waves into two perpendicularly polarized waves that propagate at different velocities. At the Earth's surface, it is therefore possible to quantify anisotropy by measuring the two splitting parameters δt and Φ. The difference in arrival times (δt) between the two split shear waves (Figure 1) depends on both the anisotropy strength

and the length of the travel path through the anisotropic medium. The azimuth Φ of the fast split shear wave polarization planes is related to the orientation of the anisotropic structure. Initially limited to direct S waves from local events (Ando and Ishikawa, 1980), the technique is now widely adopted for core-transiting phases such as SKS, SKKS, and PKS (e.g., Vinnik et al., 1984, 1989; Silver and Chan, 1991; see Savage, 1999 and Fouch and Rondenay, 2006 for a review). Travelling on nearly vertical paths, teleseismic shear-waves provide measurements of anisotropy beneath a seismic station with a relatively good lateral resolution of few tens of kilometers (Fresnel-zone width) but with poor vertical resolution. The teleseismic shear-wave splitting technique has become popular in the last decades for performing anisotropy measurements that help revealing present or past mantle deformation processes. This technique has been widely applied in several geologic settings: Subduction zones (e.g., Levin et al., 2004; Margheriti et al., 2003; Nakajima and Hasegawa, 2004), rifts (e.g., Kendall, 1994; Gao et al., 1997; Walker et al., 2004; Kendall et al., 2005), hotspots (e.g., Barruol and Granet, 2002; Walker et al., 2001; 2005), oceanic islands (e.g., Behn et al., 2004; Fontaine et al., 2005, 2007), orogens (e.g., Barruol et al., 1998; Flesch et al., 2005) and stable continental environments (e.g., Fouch et al., 2000; Heintz and Kennett, 2005; Fouch and Rondenay, 2006; Assumpção et al. 2006).

Azimuthal anisotropy was initially deduced from surface waves by Forsyth (1975), then by Nishimura and Forsyth (1988) in Pacific and by Montagner and Tanimoto (1991) at global scale. The ever-growing dataset of seismic stations and recordings have allowed, over the years, to significantly improve spatial resolution of azimuthally anisotropic tomographic models (e.g., Trampert and Woodhouse, 2003; Smith et al., 2004; Debayle et al., 2005; Maggi et al., 2006). By using the surface wave (Rayleigh and Love) frequency dependence on their penetration depth, surface wave tomography provides a relatively good vertical resolution of velocities and anisotropy down to the transition zone although the lateral resolution is relatively poor, generally not better than several hundreds of kilometres. In addition to the good vertical resolution, surface wave tomography has the advantage of providing a continuous and global-scale coverage of azimuthal anisotropy, except in poorly covered areas. This is in sharp contrast to the resolution of

81 teleseismic shear-wave splitting measurements which provide localized measures of anisotropy
82 directly beneath a seismic station.

83 Given the constraints on deformation within the Earth that seismic anisotropy offers, there is much
84 interest in understanding the origin of that anisotropy. Comparing observed fast directions with
85 absolute plate motion directions is of interest (e.g., Vinnik et al., 1984; Silver and Chan, 1991;
86 Montagner, 1994), since anisotropy in the asthenosphere, if caused by relative motion between
87 plates and deeper interior of the Earth, should have fast directions parallel to plate motion. On the
88 other hand, fossil anisotropy in the lithosphere does not need to show a correlation with current
89 plate motion directions. It is also of interest to compare seismic anisotropy with predicted seismic
90 anisotropy from flow calculations that have become available in recent years. That has been done
91 at regional scale (Griot et al., 1998; Fouch et al., 2000; Becker et al., 2006), and also at global
92 scale (Behn, et al., 2004; Becker et al., 2007; Conrad et al., 2007).

93 This study addresses the question whether shear-wave splitting observations and surface wave
94 azimuthal anisotropy can be used interchangeably for the comparison with flow models. The
95 different spatial resolution of the two types of data may result in significant differences: surface
96 waves offer vertical resolution, while body waves offer lateral resolution. Furthermore, shear-wave
97 splitting observations have mostly been made on continents (Figure 1), whereas surface wave
98 models offer some resolution at all places of the Earth's surface, although poor ray coverage may
99 result in weak constrains in some regions. A further complication for comparing the two datasets
100 arises from the fact that the anisotropy is mainly characterised by two parameters, fast orientation
101 and strength. A good coherence in one parameter does not necessarily means a good coherence in
102 the other.

103 So far, there have been only few attempts to directly relate body-wave and surface wave
104 anisotropy. Because the two techniques sample the anisotropy along vertical and horizontal
105 propagation directions, respectively, the results cannot be compared directly. Montagner, et al.
106 (2000) proposed to predict splitting parameters from a multi-layer anisotropic surface wave model.
107 That study has suggested reasonable correlation at regional scale in some regions, but at global

scale there did not appear to be a clear correlation. The possibility was discussed that the spatial resolution of the two techniques is perhaps too different to allow realistic comparisons.

In this paper we follow the approach of Montagner et al. (2000), and we study the relation between anisotropy measures from shear-wave splitting and surface wave models at global scale, as well as for a few selected key regions. We will in fact show that there is indeed a correlation at global scale, and discuss its implications. In the first part of the paper, we present the new shear-wave splitting dataset. In the second part we present the prediction of splitting measurements obtained from recent surface wave tomography and in the third part, we compare the observed splitting data with the predicted parameters.

2. World-wide shear-wave splitting results

Over the past decades, a large number of shear-wave splitting studies have been published. Some of these studies have analyzed sets of globally distributed stations (e.g. Silver, 1996; Barruol and Hoffmann, 1999), while most focused on regional networks of stations, providing detailed knowledge on specific areas. Ever-larger temporary seismic arrays (e.g. USArray) and long-running permanent stations make the available shear-wave splitting dataset grow rapidly, and the need for a central depository for all available splitting measurements has been evoked (e.g., Fouch and Rondenay, 2006). Evans et al., (2006) present a shear wave splitting database, where they re-calculated available broadband stations. Our approach is different from that. In order to make all the published splitting data easily available in a homogeneous format, we developed an interactive database. The main features of this shear-wave splitting database are that the user may: i) Enter new splitting data via a web interface, ii) Search the database for a specific station or within a region, iii) Download the whole splitting parameters and corresponding bibliographic references and iv) Visualize the database, e.g. through GoogleEarth. Such an approach ensures that results of individual studies will be taken into account by the community, as users of splitting data will

always find the most "up-to-date" information. This database is available on the "Geosciences Montpellier" website at the address http://www.gm.univ-montp2.fr/splitting/DB .

As of June 2008, the database contains 2566 entries from 133 referenced studies (see Figure 2a). Note that the database is a collection of the work of various authors over many years, using a broad range of filters and possibly quality control factors. The global splitting delay times show an approximately log-normal distribution with most values between 0.4 and 1.4 sec and a maximum at 1 sec (Figure 3a, b). This distribution is in agreement with earlier studies, e.g. that of Silver (1996). Petrophysical analyses of upper mantle rocks sampled in orogenic or ophiolite peridotite massifs, or as kimberlite or basalt xenoliths suggest that such a mean delay time requires a 100 to 150 km thick anisotropic layer (Mainprice and Silver 1993, Ben Ismail and Mainprice, 1998; Mainprice et al., 2000, Ben Ismail et al., 2001). We note that fast-axis orientations prefer E-W orientations, which are interesting in the light of speculations of uniform global plate motion relative to the underlying mantle (Doglioni, 1994; Steinberger and O'Connell, 1998; Doglioni et al., 2003). However, these statistics have to be considered with care, for two reasons: i) The ocean-continent discrepancy: Most splitting data originated from continents, where the azimuth may be dominated by frozen-in lithospheric anisotropy. Only a small amount of splitting data originated from oceanic environments where one could expect to observe present-day processes related to asthenospheric flow. ii) Seismic stations are not evenly distributed worldwide. Temporary experiments generally gather many instruments in a small area (e.g., Barruol et al., 1998; Walker et al., 2005; Flesch et al., 2005), which may cause a bias in statistical analyses. Furthermore, the different continents are not equally well sampled, and there is indeed an over-representation of North America and Western Europe in the dataset.

3. Predicting shear-wave splitting parameters from surface wave data

Montagner et al. (2000) developed a method to predict splitting parameters from surface-wave anisotropy results. Their approach is not unlike that of several earlier studies that discuss the effect

159 of multiple anisotropic layers on the effective splitting parameters (Silver and Savage, 1994;
160 Wolfe and Silver, 1998; Rümpker and Silver, 1998; Saltzer et al., 2000). The fast axis Φ as well as
161 the delay time δt of a vertically propagating SKS phase that results from a (weak) anisotropic layer
162 is related to the elastic parameters $G_s = C_{45}$, $G_c = \frac{1}{2}(C_{55} - C_{44})$, and $L = \frac{1}{2}(C_{44} + C_{55})$ that
163 can be obtained from surface wave studies (Montagner, 1986). This can be generalized for
164 multiple layers. Montagner et al. (2000) have proposed a first-order expansion that is valid at
165 periods larger than 10 seconds, e.g. for SKS and SKKS waves. Under that assumption, splitting
166 delay and fast direction can be predicted by a simple integration along the (assumed vertical) ray
167 path, as

168

$$d\bar{t} = \sqrt{\left(\int_0^a \sqrt{\frac{\rho}{L}\frac{G_c}{L}}dz\right)^2 + \left(\int_0^a \sqrt{\frac{\rho}{L}\frac{G_s}{L}}dz\right)^2}$$

169 $$\bar{\phi}_{fast} = \tfrac{1}{2}\arctan\left(\frac{\int_0^a \sqrt{\frac{\rho}{L}\frac{G_S}{L}}dz}{\int_0^a \sqrt{\frac{\rho}{L}\frac{G_C}{L}}dz}\right) \qquad (1)$$

170 where *a* corresponds to the maximum depth extent of the tomographic model and *ρ* is the density
171 of each layer. In the following we will use the global tomographic model of Debayle et al. (2005).
172 Figure 2b shows predicted shear-wave splitting for that model, integrating from 500 km to 50 km
173 depth (thus excluding the negligible influence of the crust).

174

175 Debayle et al. (2005) have used observations of fundamental and higher-mode Rayleigh waves,
176 and among the 100779 ray paths, they include many short epicentre-station paths, which give
177 particularly strong constraints. The inversion has used a spatially variable cell size determined
178 using Voronoi tessellation, and the smallest cells have sizes of about 200 km. Since anisotropic
179 and isotropic variations often occur together, it is not likely that the very small variations are
180 resolved. Therefore, the tomographic inversion has also imposed a spatial smoothness constraint
181 via a Gaussian correlation function with standard deviation of 400 km. It is clear that resolution

must vary strongly with location along the Earth's surface, due to the variable ray coverage. In places where the coverage is particularly good, resolution will be better, but it is not quite clear what the resolution limit is. In principle, a Voronoi technique is well-adapted for optimally extracting information in this situation. In any case, a lower bound on resolution is imposed by the smoothness constraint corresponding to length scales of 400 km.

Figure 3c-f presents the statistical distribution of the predicted splitting parameters. The delay times range between 0 and 2 s, with a maximum of the distribution around 0.5 s, for both continental and oceanic environments. The predicted splitting delay times are thus systematically smaller delay than the observed ones (Figure 3a, b). Potential causes for this bias may be i) the damping that is necessarily applied during the surface-wave inversion, leading to an underestimation of parameters, ii) an underestimation of true lateral variations due to an insufficient lateral resolution of surface waves and/or iii) incompatibilities between the assumptions of anisotropy systems inherent to both methods. We choose to show the angular distribution separately for continental (Figure 3c, d) and oceanic regions (Figure 3e,f). For oceanic environments, the predicted splitting orientations display hardly any azimuthal preference on a global scale. However, for continental areas there are two maxima of predicted fast directions, a stronger one in N-S direction, and a weaker one in E-W direction. The N-S predicted fast directions appear primarily in Africa, north-east Asia, and Australia (Figure 2b), where station coverage for observed splitting measurements is poor. Such a discrepancy between predicted and observed fast split direction statistics could therefore be related to the extremely uneven station coverage present in the splitting database. However, at least for Africa, the N-S orientation is in accordance with recent surface wave tomographic models (Sebai et al.; 2006; Montagner et al., 2007). The E-W maximum is much less pronounced for surface waves than that for body waves, and it therefore does not serve to confirm this as a continental feature at the largest scale.

4. Comparing observed and predicted SKS splitting

The two datasets we compare have rather different distribution on the Earth's surface. While the splitting parameters are obtained at unevenly distributed seismic stations (Figure 2a), the predicted splitting values from the surface wave model of Debayle et al. (2005) are evenly distributed on a 1ºx1º grid (Figure 2b). Comparing the two datasets therefore requires interpolation. Interpolating sparse vectorial data as splitting measurements onto a regular grid is possible (Bird and Li, 1996; Lucente et al., 2006), but to avoid stability problems due to the different spatial support, we prefer to follow the approach proposed by Montagner et al. (2000), i.e., we linearly interpolate the regular grid of the predicted anisotropy parameters to the location of each splitting measurement.

The correlation between the observed and predicted datasets is then obtained by using an adapted form of the coherence function initially defined by Griot et al. (1998). This mathematical function quantifies the correlation between two vectorial data sets on a sphere (co-latitude Θ, longitude Ψ) by taking into account the two anisotropy parameter pairs (Φ_1, δt_1; Φ_2, δt_2). Since each parameter pair corresponds to a phase and amplitude, a natural form of the coherence between two continuous fields on the sphere is

$$C(\alpha) = \frac{\iint_{\Theta\,\Psi} \left\{ dt_1(\Theta,\Psi) * \sin\Theta * dt_2(\Theta,\Psi) * \sin\Theta * \exp\left(-\frac{\left(\phi_1(\Theta,\Psi) - \phi_2(\Theta,\Psi) + \alpha\right)^2}{2D_{corr}^2} \right) \right\} d\Theta d\Psi}{\sqrt{\iint_{\Theta\,\Psi} dt_1(\Theta,\Psi)^2 * \sin^2\Theta d\Theta d\Psi} \sqrt{\iint_{\Theta\,\Psi} dt_2(\Theta,\Psi)^2 * \sin^2\Theta d\Theta d\Psi}} \quad (2)$$

The phases (fast directions) enter through an exponential form that is normalized by a "correlation factor" D_{corr}. This formula does not require an alignment of the two sets of fast axes. The test orientation α can vary between -90º and +90º and allows testing for an angular bias between the two datasets. The normalization in the conventional fashion ensures that the coherence varies between 0 (uncorrelated) to 1 (perfect correlation). An anti-correlation between the fast axes would show up as a peak at +/- 90 º.

If $C(\alpha)$ is represented by a horizontal line, the two models are uncorrelated. A Gaussian shape of $C(\alpha)$ indicates a certain coherence, with the location of the peak corresponding to the mean rotation between the models. Figure 4a illustrates this by comparing the 1°x1° predicted splitting dataset with itself. As expected, this results in a Gaussian distribution with a maximum value of 1 oriented at 0°. Figure 4b shows the coherence of the predicted splitting data on a 1° grid with that of a 10° grid. Maximum values are considerably smaller than 1 now, and the distributions are much wider, reflecting the added variance from the interpolation using the 10º grid. In fact, there is much variation of predicted fast directions in Figure 2b, at scales below 10º.

4.1. Global correlation of splitting parameters

Montagner et al. (2000) compared splitting parameters as predicted by a global anisotropic tomography model (Montagner and Tanimoto, 1991) with the shear-wave splitting results compiled by Silver (1996). The results suggested a fairly good coherence at regional scale (for instance in the Western United States and in Central Asia), but no clear coherence at global scale. The authors have attributed the latter to the different depth and lateral sensitivity in both datasets. Surface waves are best resolved in oceanic environment, where large-scale structures are expected but where station coverage and therefore shear-wave splitting measurements are sparsely distributed in that environment. In contrast, shear-wave splitting has a relatively good lateral resolution and may evidence short scale variations in upper mantle structures beneath the continents that are hardly visible from surface wave analyses. The authors also suggested that the usually-performed single-layer inversion for splitting parameters may represent an oversimplification that contributes to the missing global correlation.

Figure 4c and d show the coherence of predicted splitting from the model of Debayle et al. (2005), integrated between 50-500km depth, with the splitting database, taking into account the entire database using gridding sizes of 1º and 10º, for the correlation lengths used previously (D_{corr} = 5, 10 or 20°). The coherence is slightly broader for the 10º grid (Figure 4d) than for the 1º grid

(Figure 4c). However, both comparisons give a rather good correlation of available splitting data and anisotropic surface wave model, with a maximum centred near 0º misfit. This indicates that the available splitting database sufficiently covers the globe, as it is insensitive to the resolution of the surface wave model.

In the former study, Montagner et al. (2000) used the anisotropic surface wave model of Montagner and Tanimoto (1991) and the splitting data collection of Silver (1996). The global coherence was found to show a local minimum at 0º misfit, with local maxima on both sides. We were able to roughly reproduce this behaviour by incorporating only the splitting measurements available before 1997 (Figure 4e). Montagner et al. (2000) concluded that there is no global correlation. In fact, Figures 4d-f suggest that the absence of correlation in that study was apparently an effect of insufficient splitting data coverage and limited spatial resolution in available surface wave models at the time. Since Fresnel zones of the commonly used SKS waves are of the order of 100 km at upper mantle depths, and since splitting parameters vary at these scale length (Figure 2a), averaging azimuthal anisotropy at scale larger than 10° introduce a too large smoothing to preserve a good coherence between the body wave pattern and the large-scale surface wave pattern.

The higher correlation of the new global set (Figure 4c) in comparison to sub-dataset of Silver (1996; Figure 4e) may on the other hand reflect the numerous regional studies performed after 1996, that concentrate a large number of stations in relatively small areas, e.g. in the Eifel region (Walker et al., 2005), and the Pyrenees (Barruol et al., 1998). This leads to regional biases. The difference suggests that we should try to eliminate the regional biases if possible, or at least eliminate the effect of the spatially varying data density where we have data. So far, all data points enter equally into the coherence, and local studies with dense station coverage will thus have a stronger effect on the coherence than sparsely instrumented areas. We address this problem by gridding the splitting data. However, standard interpolation procedures are inappropriate when interpolating sparse directional data on a sphere (Bird and Li., 1996). One approach to solve this problem may be by using Voronoi cells, similar to the method of Debayle et al. (2005) or Larmat

et al. (2006). In this study, however, we follow a different approach: To account for both the amplitude and orientation of anisotropy we separate amplitude (delay time) and orientation (fast direction). The delay time is gridded using a standard cubic spline interpolation to give a map of gridded delay times *T*. The directional component of anisotropy is computed using an algorithm that has already been successfully applied to global stress data (Müller et al., 2003). The gridding algorithm is based on Watson (1985) and extended by a distance-weighting (Wehrle, 1998). For a series of unit vectors $\vec{y}$, given at positions $\vec{x}$, Watson (1985) proposes a technique that searches for a 'predictor' function $\vec{f}(\vec{x})$ that describes the vector field parallel (or anti-parallel) to $\vec{y}$. This is achieved by maximising the (quadratic) scalar product $P = \left\langle \vec{f}(\vec{x}_i)^T \vec{y}_i \right\rangle^2$. Furthermore, to be smooth, the (quadratic) scalar product of two neighbouring functions $N = \left\langle \vec{f}(\vec{x}_i)^T \vec{y}_j \right\rangle^2$ must be maximum as well. The resulting gridded vector field is thus the maximum of the following function *K(f)*:

$$K(f) = \sum_{i=1}^{n} \left(Pd(\vec{x}_i, \vec{x}_i) + \lambda \sum_{j=1, j \neq i} Nd(\vec{x}_j, \vec{x}_i) \right) \quad (3)$$

As mentioned, the P-term achieves optimum fitting of the data, the N-term controls the smoothness of the resulting field. The weighting factor λ lambda thus controls the relative influence of the data fidelity and smoothness, respectively. The function $d(x_i, x_j)$ expresses the distance weighting of point x_j at x_i within a search radius R (Wehrle, 1998). The interpolated splitting "vector field" is then the linear combination of the gridded splitting amplitude and *K(f)*, calculated at the locations $\vec{s}_i$. These coincide with the grid points of the tomographic model and thus the location of the predicted splitting parameters.

$$V = T\big|_{\vec{S}} * K(f)\big|_{\vec{S}} \quad (4)$$

Figure 5 shows an example result of that gridding for R = 600 km and λ = 5 on a 3° x 3° grid. Null measurements, though important to constrain fast directions at individual stations (Wüstefeld and Bokelmann, 2007), are not taken into account.

Similar to Figure 4, we calculate the coherence functions of the predicted splitting with these smoothed global datasets, to ascertain that the correlation between observed and predicted splitting as described in the previous section, is not an artefact of the rather heterogeneous data density. If the correlation is real, this helps to define the inherent lateral resolvability of anisotropy by the used surface-wave model.

The results for various parameter combinations of R and λ are presented in Figure 6a (D_{corr} is fixed to 10°). For all tests, there is a maximum near 0°, suggesting that there is indeed a correlation also for the gridded data, similar to the global correlation found previously (Figure 4). The correlation between the two datasets is therefore not an artefact of the uneven sampling.

Figure 6b shows the dependence of the coherence value at 0° on search radius for various λ. Interestingly, the coherence decreases clearly below R = 400km while it stays more or less constant between 400 and 1000 km. Below R = 400km, the coherence shows a weak dependence on smoothing parameter λ. This is as expected, since the effect of λ must be somewhat similar to that of the search radius. Thus, the decrease of coherence below R = 400km also manifests itself in the λ values. A peak in coherence is obtained for strong smoothing with λ = 10 and 50 at search radii of R = 400 km. Moreover, a plateau of relatively good coherence is found for λ = 5 and R between 600 and 700 km.

Figures 6c and 6d are similar to 6a and 6b, but the order of each parameter (Φ_1, δt_1; Φ_2, δt_2) has been randomised. In such random test any spatial coherence should be eliminated, unless there is an inherent correlation, due to a non-random data distribution. Comparing Figure 6c with Figure 6a we note that coherence indeed drops sharply, indicating that the correlation observed in Figure 6a is indeed real. The weak residual coherence in Figure 3b thus shows the artefact of the non-uniform distribution of splitting fast directions.

4.2. Regional correlation of splitting parameters

The previous section showed that anisotropy as determined from surface waves and those from body waves show similar results on a global scale, though both methods sample the Earth at

different scales. In this section we discuss several regional subsets of different tectonic background. Montagner et al. (2000) point out that several regional subsets have a rather good coherence despite the poor global coherence obtained in their earlier study. They relate that partially to an increased resolution of regional tomographic models used. We limit our comparison here to regional subsets of the global model. Regional tomographic models might provide higher resolution, yet a detailed comparison of all available models would be beyond the scope of this study. Figure 7 illustrates the coherence function for several regional subsets in different tectonic settings (subduction, rifts, volcanic islands, cratons). See Figures 2 and 5 for locations. Generally, the coherence is very good, with a clear maximum centred close to 0° misfit. Only the absolute value of that maximum varies between the regions. We attribute this to differences in the observed and predicted delay times, as we will discuss below.

Montagner et al. (2002) selected Western United States and Central Asia for closer discussion. For consistency and comparison with that study we will briefly discuss the results of our new coherence study, and also present results for other selected regions and tectonic settings. Additional maps of test regions can be found in the Appendix. This section shall provide an overview on coherences between the two datasets. For detailed interpretation of the anisotropy in the selected regions we kindly refer to the according publications.

4.2.1. The Andes

Several studies analysed shear-wave splitting in the Andes and adjacent Nazca plate. Polet et al. (2000) argue that most significant contribution to splitting occurs below the slab, with a complex, spatially varying anisotropy pattern. Russo and Silver (1994) and Helffrich et al. (2002) propose that the large-scale pacific mantle flow pattern is deviated around the South American continent by roll-back of the Nazca slab.

The coherence between predicted and interpolated observed splitting is variable in this area, with poles at -70°, +20° and +60° (Figure 7a, Figure A1). This behaviour renders the complex interaction, sometimes at small scale, between subduction of oceanic plate and mountain range

359 formation, both of which may cause different anisotropy orientations (Vauchez and Nicolas, 1991;
360 Barruol et al., 1998; Kneller et al., 2007).

361 4.2.2. The East Pacific Rise

362 The coherence between predicted and interpolated observation of splitting is striking for stations in
363 the vicinity of the East Pacific Rise (Figure 7b; Figure A2). These measurements come from the
364 MELT and GLIMPSE Ocean Bottom Seismometers experiments (Wolfe and Solomon, 1999;
365 Harmon et al., 2004). They proposed Lattice Preferred Orientation (LPO) of anisotropic minerals
366 parallel to mantle flow trending normal to the spreading axis as main cause for splitting, as well as
367 a deeper contribution of an asthenospheric return flow from the South Pacific superswell. This
368 agreement between the fast split directions and the surface wave anisotropy is not restricted to the
369 ridge itself but is extending further West in the French Polynesia domain where Fontaine et al.
370 (2007) evidenced a clear signature of the asthenospheric flow in the SKS splitting observations
371 that also dominates within the surface wave tomographies, both exhibiting dominant fast directions
372 parallel to the plate motion direction. Further south, the EPR region also contains station RPN,
373 located on the Easter Island Hot Spot, for which a multilayer case has been proposed (Fontaine et
374 al., 2007). The SKS anisotropy pattern observed at this station is clearly not the result of the ridge
375 spreading alone and may likely result from the combination of spreading-related mantle flow and
376 hotspot-related mantle upwelling. South and east of station RPN, although both the station
377 coverage and resolution of the surface wave model is too small to confidently relate this behaviour
378 to mantle upwelling, the predicted and interpolated splitting coincide rather well, whereas towards
379 the north, the two models are almost perpendicular. This can be seen in Figure 7b as a smaller
380 peak at -65°.

381 *4.2.3. North America*

382 The understanding of regional tectonics in North America is continuously improved (e.g.,
383 Humphreys and Coblentz, 2007). Seismic anisotropy beneath North America has been addressed
384 by numerous authors (see references in Walker et al., 2004; Fouch and Rondenay, 2006,
385 Bokelmann and Wüstefeld, 2009). The pertaining mantle flow is mainly controlled by the various

386 tectonic settings ranging from cratons in the north (e.g., Bokelmann, 2002a, b), mountain ranges in
387 the east (e.g., Barruol et al., 1997; Fouch et al., 2000), and continental hotspot (e.g., Waite et al.,
388 2005) and subduction in the west that could interfere with strike-slip tectonics to produce a
389 complex toroidal mantle flow pattern (e.g., Xue and Allen, 2007; Zandt and Humphreys, 2008).
390 The splitting dataset presented in this study indicates good correlation with the splitting predicted
391 from surface wave azimuthal anisotropy in North America (Figure 7c, Figure A3). Montagner et
392 al. (2000) observed however a rotation of +30º between observed and predicted splitting in the
393 Western US (Figure 8a). In this region, the coherence of the new dataset has improved (Figure 7d),
394 likely due to the larger amount of splitting data (109 measurements today versus 47 available in
395 1996), but perhaps also due to the more recent tomographic model used in this study that may
396 provide an improved lateral resolution. The resulting misfit is reduced to a slight rotation of -10º
397 for all of North America. In Western North America the angular misfit is precisely 0º. This
398 suggests that surface waves and shear wave splitting experience the same anisotropic structures
399 (Figure 8a) and therefore, that the apparent complexity of the crustal tectonics in this region may
400 be overlying a mantle structure characterized by a simpler pattern at longer wavelength. It thus
401 appears to be consistent to invert the two datasets together as has been done recently by Marone
402 and Romanowicz (2007).

403 4.2.4. Kaapvaal Craton

404 Several studies analysed the Kaapvaal upper mantle anisotropy by using either SKS wave splitting
405 (e.g., Vinnik et al., 1996; Barruol and Ben Ismail, 2001; Silver et al., 2001; Fouch et al., 2004) or
406 the information brought to the surface by kimberlite nodules (e.g., Ben Ismail et al., 2001). Silver
407 et al. (2001) and Gao et al. (2002) point out that the fast orientations do not correlate with plate
408 motion directions of Gripp and Gordon (2002). The fast orientation correlates however very well
409 with regional geologic trends, suggesting lithospheric origins of anisotropy. Furthermore, a high-
410 density array in the Kimberley region found small-scale variations in shear wave splitting
411 parameters, which can only be explained by lithospheric origins of anisotropy (Fouch et al., 2004).

In global tomographic models, one of the most intriguing features is the African Superswell (e.g., Nyblade and Robinson, 1994; Ritsema and van Heijst, 2000; Conrad and Gurnis, 2003), which is an ongoing, large-scale, northward oriented mantle upwelling. This upwelling can provide an explanation for the predicted splitting (Figure 2b, 8b) particularly because of the absence of predicted splitting beneath the Namibia-Botswana border region (Figure 8b), since vertically oriented anisotropy is not included in the methods used here. The presence of two peaks in the regional coherence function (Figure 7e) may indicate that the anisotropy observed by tomographic studies is not only related to the ongoing mantle upwelling, but also related to ancient lithospheric anisotropy, at least in the upper mantle regions.

4.2.5. The East African Rift Zone

Rifting along the East African Rift Valley (EAR) has been analysed at mantle to crustal scales by various studies (see Kendall et al., 2006 for a review). Collectively, the results support a model for magma assisted rifting in Ethiopia with an increase in melt production towards the Red Sea, which is strongly supported by the prediction of partial melt on the basis of P- and S-wave tomography (Bastow et al., 2005, 2008). In Tanzania and Kenya, fast split shear waves parallel the E and W arms of the EAR that encircle the Tanzanian craton (Gao et al., 1997; Walker et al., 2004).

The coherence between observed and predicted splitting is rather strong with a maximum at 0° deviation (Figure 7f, Figure A4). The strong coherence is mainly due to high correlation of both direction and amplitude of splitting between the predicted and interpolated datasets beneath Afar (Figure A4). Kendall et al. (2006) proposed a suite of different causes of anisotropy beneath the East African rift system. The main cause of anisotropy is attributed to thin melt pockets directly beneath the rift zone, oriented parallel to the rift axis. Away from the rift axis, the lithospheric LPO is likely related to pre-existing fabric, while beneath the lithosphere the LPO could be due to viscous coupling between the base of the lithosphere and large-scale mantle upwelling. This model explains the rift-parallel fast splitting orientations in the rift valley. Such explanation leaves the good correlation somewhat surprising, since global surface waves are not expected to resolve that feature. The splitting delay times predicted in this area are relatively low, which may be due to two

perpendicular anisotropic orientations (see discussion for Australia). An alternative explanation might be that the mantle upwelling beneath the rift causes vertically oriented fast axis in the mantle. These do not contribute to the observed and the predicted splitting.

4.2.6. Central Asia

In Central Asia (Figure 7g, Figure A5), more than 250 measurements are now available, in comparison with the 33 available before 1997. The new model seems to be less coherent (Figure 7g) than the previous one, as discussed in Montagner (2000), and it is characterized by the presence of two peaks in the coherence function at +15º and -70 º. Montagner et al. (2000) used a local high-resolution tomographic model (Griot et al., 1998) for calculating the predicted splitting. The two compared datasets seem to be rotated by 20°. The main region of discrepancy is the Tibetan Plateau, while coherence is good for the Tien Shan basin in the North-West and the North China craton, in the North-East of Figure A5). In general, discrepancies between the global (Montagner and Tanimoto, 1991) and local (Griot et al, 1998) tomographic datasets highlight the importance of local high-resolution tomography that may be sensitive to shorter wavelength structures. This regional analysis also suggests that more data do not necessarily imply a better coherence since local studies involving a large number of stations over a limited space may strongly bias the general coherence function at the regional and global scale. They conclude that future approaches should consider the effect of different data density in greater detail. New azimuthal anisotropy tomographic models of Central Asia with an enhanced lateral resolution are presently issuing. Consequently time is ripe for a new quantitative comparison between SKS splitting data and tomographic models, but it is beyond the scope of this paper.

4.2.7 Australia

The coherence in Australia is rather good (Figure 7h, A6). Given the complex anisotropy described by other studies of this area, this is somewhat surprising. Debayle et al. (2005) found that Australia is the only continent where azimuthal anisotropy (inferred from surface waves)

correlates well with present day absolute plate motion. This correlation is most significant at depths between 150 and 300km. In Australia many stations are observed as isotropic, i.e. Nulls from a broad range of backazimuths. Heintz and Kennett (2005, 2006) point out that this apparent isotropy at these stations is also consistent with two layers of mutually perpendicular anisotropy orientations (Silver and Savage, 1994; Barruol and Hoffmann, 1999).

The predicted shear wave splitting contains a few regions of negligible splitting amplitude (central Northern Territory, just south of Western Australia, and in Central New South Wales; see Figure A6). In our approach, the predicted splitting is calculated from 19 layers, each 25 km thick. The correlation between non-Null observations and predicted splitting is very good, indicating that such gradual change in anisotropy orientation with depth mimics the non-Null splitting observations well. This in turn indicates that assuming a two layer case may be an oversimplification.

5. Discussion

Generally, the resolution of global anisotropic surface wave models is thought to not be better than a thousand kilometres. For an increasing number of regions, recent high-resolution regional anisotropic tomographic models are available, and future studies should address their correlation with regional splitting data in more detail. For the global model, the dependence of correlation on search radius in Figure 6b may suggest that resolution capability is somewhat better than the initially thought thousand kilometres. This is true at least for the parts of the Earth that contain the most seismological stations. These areas correspond to the seismically best-resolved portions on Earth, obviously for shear wave splitting but also in surface wave data due to the higher density of crossing ray paths in those areas. The use of Voronoi cells allows the tomographic model of Debayle et al. (2005) to reflect spatially varying resolutions. The drop-off in correlation below 400 km is interesting, since we would be able to see that effect only if there is resolution of surface wave data for those best-resolved parts of the Earth down to 400 km length scales, which is considerably better than we expected. Whether or not this is the correct explanation for the decay below 400 km, this resolution study is very encouraging, since it indicates lateral surface wave

492 resolution somewhat below a thousand kilometres for the well-resolved portion of the Earth. The
493 resolution will be considerably weaker in less well-covered regions. A recent study of the
494 Canadian shield (Bokelmann and Wüstefeld, 2009) has suggested that surface-wave anisotropy
495 models do not yet have a similar resolution there, which would be required to distinguish inner-
496 cratonic variations of anisotropy.

497 This will probably change somewhat in the next years, with the availability of massive regional
498 datasets. Also methodological developments such as simultaneous inversions of splitting and
499 surface wave data are quite useful (e.g., Marone and Romanowicz, 2007).

500 A limitation of our method is that no Null stations, i.e. apparently isotropic stations, are included.
501 The explanation of such Null stations is not yet completely understood as ever more evidence
502 suggests that at least the upper part of the mantle is anisotropic. This evidence is based on
503 seismological observations as presented in this paper and also on mineralogical studies (e.g., Ben
504 Ismail and Mainprice, 1998; Mainprice et al., 2000; Holtzman et al., 2003). Nulls stations do not
505 necessarily imply pervasive upper mantle isotropy, but may for example be caused by two
506 anisotropic layers with mutually perpendicular fast orientations (e.g., Silver and Savage, 1994;
507 Heintz and Kennett, 2006). Null stations may also not imply large scale upper mantle isotropy. For
508 instance, P-polarization analysis at station PPT in Tahiti Island (Fontaine et al., 2009) clearly
509 demonstrates that the isotropy deduced from SKS splitting, located vertically beneath the station,
510 has a restricted lateral extent, implying that such a short-scale upper mantle structure can hardly be
511 visible in surface wave tomographies.

512 The database contains only a limited amount of multi-layer cases. For the bulk of data, the
513 observed (apparent) splitting parameters reflect the vertical integration of the different layers of the
514 surface wave anisotropic model Although the model is divided in 19 layers between 40 and 500
515 km depth, the radial correlation length limits the actual number of independent layers to 4 or 5.
516 These layers can in turn display effectively the same azimuth and so the real number of layers with
517 different orientations (in complex areas) may be at the most two or three. However, it is important
518 to note that in many areas these azimuthal variations and this stratification of anisotropy are real

519 and significant, although they cannot directly be inferred from shear wave splitting (Silver and
520 Savage, 1994; Rümpker and Silver, 1998; Saltzer et al., 2000).

521 The predicted delay times are smaller than the observed. Figure 9 shows a scatter-plot, comparing
522 the predicted delay times of the surface wave model with those delay times of the smoothed,
523 observed delay times for smoothing parameters of R = 600 km. The majority of the data are
524 located on the right-hand side of the graph, implying that surface wave-predicted delay times are
525 biased to smaller values. This also shows up in relatively low coherence (Figure 4). Our findings
526 of best coherence between the two datasets at approximately 600 km is in agreement with the
527 stochastic model of anisotropy correlation by Becker et al. (2007), which reveals a relatively short
528 correlation length of splitting parameters of L ~550 km for orogens and volcanic zones.

529 There is only a limited amount of shear-wave splitting measurements in the oceans although future
530 deployments of Ocean Bottom Seismometers will eventually enhance the global splitting coverage
531 (e.g., Suetsugu et al., 2005). This should allow for a separate analysis of continents having mostly
532 thick and old lithosphere, with sometimes ancient anisotropy orientations, and oceans having a
533 much more recent and simpler history (Montagner, 2002; Becker et al., 2003), which will probably
534 include exciting new possibilities such as observing hotspot-induced mantle flow, small-scale
535 convection, plume-ridge interaction etc.

536 The coverage of shear-wave splitting data that are available at this point does not allow accepting
537 or rejecting predominantly East-West mantle flow (e.g., Doglioni, 1994) at global scale as
538 manifested in fast directions. The maximum observed in Figure 3b is clearly an artefact of the
539 spatial sampling and probably includes many observations of fossil lithospheric anisotropy.

540 **6. Conclusion**

541 In this paper, we have compared shear-wave splitting measurements made around the world with
542 predicted splitting parameters derived from anisotropic surface wave tomography. This allowed us
543 to show that the two measures of anisotropy are indeed correlated, even though they have very
544 different lateral and vertical resolution. This correlation is apparently supported by the fact that

both measures are mostly sensitive to the upper mantle (e.g., Sieminski et al., 2007). The quality of the measurements and resulting models allows us to address the limit of lateral resolution of the anisotropic surface wave model. Finally, the agreement of the two different methods highlights the fact that the two techniques are fully complementary since they are sensitive to vertical or lateral variations of upper mantle flow and therefore deserve to be twined together in studies aiming at mapping upper mantle deformation.

Acknowlegdements

We would like to thank Derek Schutt and Matt Fouch for their initial work of collecting the splitting parameters and for providing them online. Alexis Rochat helped us entering additional SKS published data. Special thank goes to all colleagues who already entered their results to the database. We are grateful to Birgit Müller and Oliver Heidbach of the University of Karlsruhe for providing the smoothing code. We thank Ian Bastow for discussion on the East African Rift. The reviews by of Matt Fouch and Christine Houser greatly improved our manuscript.

559 **References**

560 Ando, M., Ishikawa, Y., Wada, H., 1980, S-wave anisotropy in the upper mantle under a volcanic
561 area in Japan, *Nature,* 286, 43–46

562 Assumpcao, M., Heintz, M., Vauchez, A., Silva, M. E., 2006, Upper mantle anisotropy in SE and
563 Central Brazil from SKS splitting: Evidence of asthenospheric flow around a cratonic keel,
564 *Earth Planet. Sci. Lett.*, 250(1-2), 224-240.

565 Babuska, V., Plomerova, J., and Sileny, J., 1984, Spatial variations of P-residuals and deep-
566 structure of the European lithosphere, *Geophys. J. Roy. Astron. Soc.,* 79(1), 363-383.

567 Backus, G. E., 1962, Long-Wave Elastic Anisotropy Produced by Horizontal Layering, *J.*
568 *Geophys. Res.*, 67(11), 4427-4440.

569 Barruol, G., Ben Ismail, W., 2001, Upper mantle anisotropy beneath the African IRIS and
570 Geoscope stations, *Geophys. J. Int.*, 146(2), 549-561, doi: 10.1046/j.0956-
571 540x.2001.01481.x

572 Barruol, G., Granet, M., 2002, A Tertiary asthenospheric flow beneath the southern French Massif
573 Central indicated by upper mantle seismic anisotropy and related to the west
574 Mediterranean extension, *Earth Planet. Sci. Let.*, 202, 31-47, doi:10.1016/S0012-
575 821X(02)00752-5.

576 Barruol, G., Hoffmann, R., 1999, Upper mantle anisotropy beneath the Geoscope stations, *J.*
577 *Geophys. Res.*, 104(B5), 10757-10773.

578 Barruol, G., Souriau, A., Vauchez, A., Diaz, J., Gallart, J., Tubia, J., Cuevas, J. (1998),
579 Lithospheric anisotropy beneath the Pyrenees from shear wave splitting, *J. Geophys. Res.*
580 103(B12), 30039-30053.

581 Barruol, G., Silver, P. G., Vauchez, A., 1997, Seismic anisotropy in the eastern US: deep structure
582 of a complex continental plate, *J. Geophys. Res.*, 102, 8329-8348

583 Bastow, I. D., Stuart, G. W., Kendall, J.M., Ebinger C. J., 2005, Upper-mantle seismic structure in
584 a region of incipient continental breakup: northern Ethiopian rift. *Geophys. J. Int.*, 162**,**
585 479-493, doi: 10.1111/j.1365-246X.2005.02666.x,

586 Bastow, I. D., Nyblade, A. A., Stuart, G. W., Rooney, T., Benoit, M. H., 2008. Upper Mantle

587 Seismic Structure Beneath the Ethiopian Hotspot: Rifting at the Edge of the African Low
588 Velocity Anomaly. *Geochem. Geophys. Geosyst.*, 9(12), Q12022,
589 doi:10.1029/2008GC002107

590 Becker, T. W., Kellogg, J. B., Ekstrom, G., O'Connell, R. J., 2003, Comparison of azimuthal
591 seismic anisotropy from surface waves and finite strain from global mantle-circulation
592 models, *Geophys. J. Int.*, 155(2), 696-714.

593 Becker, T. W., Browaeys, J. T., Jordan, T. H., 2007, Stochastic analysis of shear-wave splitting
594 length scales, *Earth Planet. Sci. Lett.*, 259, 526-540.

595 Becker, T. W., Chevrot, S., Schulte-Pelkum, V., Blackman, D. K., 2006, Statistical properties of
596 seismic anisotropy predicted by upper mantle geodynamic models, *J. Geophys. Res.*
597 111(B10), B08309

598 Behn, M. D., Conrad, C. P., Silver, P., 2004, Detection of upper mantle flow associated with the
599 African Superplume, *Earth Planet. Sci. Lett.,* 224, 259-274.

600 Ben-Ismail, W., Barruol, G., Mainprice, D., 2001, The Kaapvaal craton seismic anisotropy:
601 Petrophysical analyses of upper mantle kimberlite nodules, *Geophys. Res. Lett.,* 28, 2497-
602 2500.

603 Ben Ismail, W., Mainprice, D., 1998, An olivine fabric database: an overview of upper mantle
604 fabrics and seismic anisotropy, *Tectonophysics,* 296(1-2), 145-157.

605 Bird, P., Li, Y., 1996, Interpolation of principal stress directions by nonparametric statistics:
606 Global maps with confidence limits, *J. Geophys. Res.,* 101, 5435-5444.

607 Bokelmann, G. H. R., 1995, P-wave array polarization analysis and effective anisotropy of the
608 brittle crust, *Geophys. J. Int.,* 120(1), 145-162.

609 Bokelmann, G. H. R., 2002a, Convection-driven motion of the North American craton: Evidence
610 from P-wave anisotropy, *Geophys. J. Int.,* 248(2), 278-287.

611 Bokelmann, G.H.R., 2002b, Which forces drive North America?, *Geology*, 30(11), 1027-1030.

612 Bokelmann, G. H. R., Wüstefeld, A., 2009, Comparing crustal and mantle fabric from the
613 North American craton using magnetics and seismic anisotropy, *Earth Planet. Sci. Lett.,*
614 *277(3-4), 355-364, doi:10.1016/j.epsl.2008.10.032*

615 Conrad, C. P., Behn, M. D., Silver, P. G., 2007, Global mantle flow and the development of
616 seismic anisotropy: Differences between the oceanic and continental upper mantle, *J.*
617 *Geophys. Res.,* 112, B07317.

618 Conrad, C. P., Gurnis, M., 2003, Seismic tomography, surface uplift, and the breakup of
619 Gondwanaland: Integrating mantle convection backwards in time, *Geochemistry,*
620 *Geophysics, Geosystems*, 4(3), 1031.

621 Crampin, S., 1984, Effective anisotropic elastic constants for wave propagation through cracked
622 solids, *Geophys. J. R. Astron. Soc.*, 76, 135-145.

623 Debayle, E., Kennett, B., Priestley, K., 2005, Global azimuthal seismic anisotropy and the unique
624 plate motion deformation of Australia, *Nature*, 433, 509-512.

625 Doglioni, C., 1994, Foredeeps versus subduction zones, *Geology*, 22(3), 271-274.

626 Doglioni, C., Carminati, E., Bonatti, E., 2003, Rift asymmetry and continental uplift, *Tectonics,*
627 22(8), 1024

628 Evans, M. S., Kendall, J., Willemann, R. J., 2006, Automated SKS splitting and upper-mantle
629 anisotropy beneath Canadian seismic stations, *Geophys. J. Int.*, 165(3), 931-942.

630 Flesch, L. M., Holt, W. E., Silver, P. G., Stephenson, M., Wang, C., Chan, W. W., 2005,
631 Constraining the extent of crust-mantle coupling in central Asia using GPS, geologic, and
632 shear wave splitting data, *Earth Planet. Sci. Lett.,* 238, 248-268.

633 Fontaine, F. R., G. Barruol, B. L. N. Kenneth, G. H. R. Bokelmann, and D. Reymond (2009),
634 Upper mantle anisotropy beneath Australia and Tahiti from P-wave polarization -
635 Implication for real-time earthquake location, *J. Geophys. Res.*, *114* (B03306),
636 doi:10.1029/2008JB005709.

637 Fontaine, F. R., Barruol, G., Tommasi, A., Bokelmann, G. H. R., 2007, Upper-mantle flow
638 beneath French Polynesia from shear wave splitting, *Geophys. J. Int.*, 170, 1262-1288, doi:
639 10.1111/j.1365-246X.2007.03475.x.

640 Fontaine, F. R., Hooft, E. E. E., Burkett, P. G., Toomey, D. R., Solomon, S. C., Silver, P. G., 2005,
641 Shear-wave splitting beneath the Galápagos archipelago, *Geophys. Res. Lett.,* 32, L21308,
642 doi:10.1111/j.1365-246X.2007.03475.x

643 Forsyth, D. W., 1975, A new method for the analysis of multi-mode surface-wave dispersion:

644 Application to Love-wave propagation in the east Pacific, *Bull. Seis. Soc. Am.,* 65(2), 323-
645 342

646 Fouch, M. J., Fischer, K. M., Parmentier, E. M., Wysession, M. E., Clarke, T. J., 2000, Shear wave
647 splitting, continental keels, and patterns of mantle flow, *J. Geophys. Res.,* 105(B3), 6255-
648 6275.

649 Fouch, M. J., Rondenay, S., 2006, Seismic anisotropy beneath stable continental interiors, *Phys.*
650 *Earth Planet. Int.*, 158(2-4), 292-320.

651 Fouch, M. J., Silver, P. G., Bell, D. R., Lee, J. N., 2004, Small-scale variations in seismic
652 anisotropy near Kimberley, South Africa, *Geophys. J. Int.,* 157, 764-774.

653 Gao, S., Davis, P. M., Liu, H., Slack, P. D., Rigor, A. W., Zorin, Y. A., Mordvinova, V. V.,
654 Kozhevnikov, V. M., Logatchev, N. A., 1997, SKS splitting beneath continental rift zones,
655 *J. Geophys. Res.*, 102(B10), 2281-22798.

656 Gao, S. S., Silver, P. G., Liu, K. H., 2002, Mantle discontinuities beneath Southern Africa,
657 *Geophys. Res. Lett.*, 29(10), 1491, doi:10.1029/2001GL013834

658 Griot, D., Montagner, J., Tapponnier, P., 1998, Phase velocity structure from Rayleigh and Love
659 waves in Tibet and its neighbouring regions, *J. Geophys. Res.,* 103, 21215-21232.

660 Gripp, A. E., Gordon, R. G., 2002, Young tracks of hotspots and current plate velocities,
661 *Geophys. J. Int.,* 150(2), 321-361, doi: 10.1046/j.1365-246X.2002.01627.x

662 Harmon, N., D. W. Forsyth, K. M. Fischer, and S. C. Webb , 2004, Variations in shear-wave
663 splitting in young Pacific seafloor, *Geophys. Res. Lett.*, 31, L15609, doi: 10.1029/2004GL020495.

664 Helffrich, G., Wiens, D. A., Vera, E., Barrientos, S., Shore, P., Robertson, S., Adaros, R., 2002, A
665 teleseismic shear-wave splitting study to investigate mantle flow around South America
666 and implications for plate-driving forces, *Geophys. J. Int.,* 149(1), F1-F7, doi:
667 10.1046/j.1365-246X.2002.01636.x

668 Heintz, M., Kennett, B. L. N., 2005, Continental scale shear wave splitting analysis: Investigation
669 of seismic anisotropy underneath the Australian continent, *Earth Planet. Sci. Lett.,* 236(1-
670 2), 106-119.

671 Heintz, M., Kennett, B. L. N., 2006, The apparently isotropic Australian upper mantle, *Geophys.*
672 *Res. Lett*., 33, L15319. doi:10.1029/2006GL026401

673 Hess, H. H., 1964, Seismic Anisotropy of the Uppermost Mantle under Oceans, *Nature,* 203, 629-
674 631.

675 Holtzman, B. K., Kohlstedt, D. L., Zimmerman, M. E., Heidelbach, F., Hiraga,T. ; Hustoft, J,
676 2003, Melt Segregation and Strain Partitioning: Implications for Seismic Anisotropy and
677 Mantle Flow, *Science,* 29(301), 1227 – 1230, doi: 10.1126/science.1087132

678 Humphreys, E. D., Coblentz, D. D., 2007, North American dynamics and western U.S. tectonics,
679 *Rev. Geophys.*, 45, RG3001, doi:10.1029/2005RG000181

680 Kendall, J. M., Pilidou, S., Keir, D., Bastow, I., Stuart, G., Ayele, A., 2006, Mantle upwellings,
681 melt migration and magma assisted rifting in Africa: Insights from seismic anisotropy. In:
682 G. Yirgu; C. J. Ebinger, P. K. H. Maguire (Editors), Structure and evolution of the rift
683 systems within the Afar volcanic province, Northeast Africa, pp. 57-74.

684 Kendall, J. M., Stuart, G., Ebinger, C., Bastow, I., Keir, D., 2005, Magma-assisted rifting in
685 Ethiopia, *Nature*, 433, 146-148.

686 Kendall, J. M., 1994, Teleseismic arrivals at a mid-ocean ridge: Effect of mantle melt and
687 anisotropy, *Geophys. Res. Lett.,* 21, 301-304.

688 Kneller, E. A., van Keken, P. E., Katayama, I., Karato, S., 2007, Stress, strain, and B-type olivine
689 fabric in the fore-arc mantle: Sensitivity tests using high-resolution steady-state
690 subduction zone models, *J. Geophys. Res*., 112(B4), B04406. doi:10.1029/2006JB0

691 Larmat, C., Montagner, J.-P., Fink, M., Capdeville, Y., Tourin, A., Clévédé E., 2006, Time-
692 reversal imaging of seismic sources and application to the great Sumatra earthquake
693 *Geophys. Res. Lett.*, 33, L19312, doi:10.1029/2006GL026336.

694 Levin, V., Droznin, D., Park, J., Gordeev, E., 2004, Detailed mapping of seismic anisotropy with
695 local shear waves in southeastern Kamchatka, *Geophys. J. Int.,* 158(3), 1009-1023.

696 Lucente, F. P., Margheriti, L., Piromallo, C., Barruol, G., 2006, Seismic anisotropy reveals the
697 long route of the slab through the western-central Mediterranean mantle, *Earth Planet. Sci.*
698 *Lett.,* 241, 517-529, doi:510.1016/j.epsl.2005.1010.1041.

699 Maggi, A., Debayle, E., Priestley, K., Barruol, G., 2006, Azimuthal anisotropy of the Pacific
700 region, *Earth Planet. Sci. Lett.,* 250, 53-71, doi: 10.1016/j.epsl.2006.07.010.

701 Mainprice, D., Barruol, G., Ben Ismail, W., 2000. The seismic anisotropy of the Earths mantle:

from single crystal to polycrystal. In: S.I. Karato, A. Forte, R.C. Liebermann, G. Masters and L. Stixrude (Editors) Earths deep interior: Mineral Physics and Tomography from the atomic to the global scale. Geophysical Monograph. AGU, Washington, D.C., vol 117, pp. 237-264.

Mainprice, D., Silver, P. G., 1993, Interpretation of SKS-waves using samples from the subcontinental lithosphere, *Phys. Earth Planet. Int.,* 78, 257-280.

Margheriti, L., Lucente, F. P., Pondrelli, S., 2003, SKS splitting measurements in the Apenninic-Tyrrhenian domain (Italy) and their relation with lithospheric subduction and mantle convection, *J. Geophys. Res.,* 108, B2218, doi:10.1029/2002JB001793.

Marone, F., Romanowicz, B., 2007, The depth distribution of azimuthal anisotropy in the continental upper mantle, *Nature,* 447(7141, 198-201.

Montagner, J.-P., Marty, B., Stutzmann, E., Sicilia, D., Cara, M., Pik, R., Lévêque, J.-J., Roult, G., Beucler, E., Debayle, E, 2007, Mantle upwellings and convective instabilities revealed by seismic tomography and helium isotope geochemistry beneath eastern Africa, *Geophys. Res. Lett*., 34, L21303, doi:10.1029/2007GL031098.

Montagner, J.-P., 1994, Can seismology tell us anything about convection in the mantle?, *Rev. Geophys., 32(2), 115-137*

Montagner, J.-P., 2002, Upper mantle low anisotropy channels below the Pacific Plate, *Earth Planet. Sci. Lett.,* 202, 263-274.

Montagner, J.-P., 1986, Dimensional structure of the Indian Ocean inferred from long period surface waves, *Geophys. Res. Lett.,* 13, 315-318.

Montagner, J.-P., Griot-Pommera, D., Lavé, J., 2000, How to relate body wave and surface wave anisotropy?, *J. Geophys. Res.,* 105, 19015-19028.

Montagner, J.-P., Tanimoto, T., 1991, Global Upper Mantle Tomography of Seismic Velocities and Anisotropies, *J. Geophys. Res.*, 96(B12), 20,337–20,351

Müller, B., Wehrle, V., Hettel, S., Sperner, B., Fuchs, K., 2003, A new method for smoothing oriented data and its application to stress data, In: M. Ameen (Editor). Fracture and in-situ stress characterisation of hydrocarbon reservoirs, Geol. Soc. Lond. Spec. Publ., pp. 107-126.

731 Nakajima, J., Hasegawa, A., 2004, Shear-wave polarization anisotropy and subduction-induced
732 flow in the mantle wedge of northeastern Japan, *Earth Planet. Sci. Lett.,* 225, 365-377.

733 Nicolas, A., Christensen, N. I., 1987, Formation of anisotropy in upper mantle peridotites - A
734 review, In: K. Fuchs, C. Froideveaux (Editors). Composition structure and dynamics of the
735 lithosphere asthenosphere system, AGU, Washington D.C., pp. 111-123.

736 Nishimura, C. E., Forsyth, D. W., 1988, Rayleigh wave phase velocities in the Pacific with
737 implications for azimuthal anisotropy and lateral heterogeneities, *Geophys. J. Int.,* 94, 479-
738 501.

739 Nyblade, A. A., Robinson, S. W., 1994, The African superswell, *Geophys. Res. Lett*., 21, 765-768.

740 Polet, J., Silver, P.G., Beck, S., Wallace, T., Zandt, G., Ruppert, S., Kind, R., Rudloff, A., 2000,
741 Shear wave anisotropy beneath the Andes from the BANJO, SEDA, and PISCO
742 experiments, *J. Geophys. Res.*, 105(B3), 6287–6304

743 Ritsema, J., van Heijst, H., 2000, New seismic model of the upper mantle beneath Africa,
744 Geology; 28(1), 63-66;

745 Rümpker, G., Silver, P. G., 1998, Apparent shear-wave splitting parameters in the presence of
746 vertically varying anisotropy, *Geophys. J. Int.*, 135(3), 790-800.

747 Russo, R.M. and Silver, P.G., 1994. Trench-parallel flow beneath the Nazca plate from seismic
748 anisotropy, *Science*, 263, 1105-1111.

749 Saltzer, R. L., Gaherty, J. B., Jordan, T. H., 2000, How are vertical shear wave splitting
750 measurements affected by variations in the orientation of azimuthal anisotropy with
751 depth?, *Geophys. J. Int.,* 141, 374-390.

752 Savage, M. K., 1999, Seismic anisotropy and mantle deformation: what have we learned from
753 shear wave splitting, *Rev. Geophys.,* 37, 69-106.Schulte-Pelkum, V., Blackman, D. K.,
754 2003, A synthesis of seismic P and S anisotropy, *Geophys. J. Int.,* 154, 166-178.

755 Schulte-Pelkum, V., Masters, G., Shearer, P. M., 2001, Upper mantle anisotropy from long-period
756 P polarization, *J. Geophys. Res.,* 106, 21917-21934.

757 Sebai, A., Stutzmann, E., Montagner, J.-P., Sicilia, D., Beucler, Eric, 2006) Anisotropic structure
758 of the African upper mantle from Rayleigh and Love wave tomography, *Phys. Earth*
759 *Planet. Int.,* 155(1-2), 48-62

760 Sieminski, A., Liu, Q., Trampert, J., Tromp, J, 2007, Finite-frequency sensitivity of body waves to
761 anisotropy based upon adjoint methods, *Geophys., J. Int.,* 171(1), 368-389,
762 doi:10.1111/j.1365-246X.2007.03528.x

763 Silver, P. G., 1996, Seismic Anisotropy Beneath the Continents: Probing the Depths of Geology,
764 *Annu. Rev. Earth Planet. Sci.,* 24, 385-432.

765 Silver, P. G., Chan, W. W., 1991, Shear Wave Splitting and Subcontinental Mantle Deformation,
766 *J. Geophys. Res.,* 96(B10), 16429-16454.

767 Silver, P. G., Savage, M., 1994, The interpretation of shear-wave splitting parameters in the
768 presence of two anisotropic layers, *Geophys. J. Int.,* 119, 949-963.

769 Silver, P. G., Gao, S. S., Liu, K. H., 2001, Mantle deformation beneath southern Africa, *Geophys.*
770 *Res. Let.,* 28(13), 2493-2496.

771 Simons, F. J., van der Hilst, R. D., 2003, Seismic and mechanical anisotropy and the past and
772 present deformation of the Australian lithosphere, *Earth Planet. Sci. Lett.*, 211(3-4), 271-
773 286 doi:10.1016/S0012-821X(03)00198-5

774 Smith, D. B., Ritzwoller, M. H., Shapiro, N. M., 2004, Stratification of anisotropy in the Pacific
775 upper mantle, *J. Geophys. Res.,* 109(B18), B11309.

776 Steinberger, B., O'Connel, R. J., 1998, Advection of plumes in mantle flow: implications for
777 hotspot motion, mantle viscosity and plume distribution, *Geophys. J. Int.* 132(2), 412-
778 434.Suetsugu, D., Isse, T., Tanaka, S., Obayashi, M., Shiobara, H., Sugioka, H.,
779 Kanazawa, T., Fukao, Y., Barruol, G., Reymond, D., 2005, Probing South Pacific mantle
780 plumes with Broadband OBS. *Eos*, 86(44): 429-435.

781 Trampert, J., Woodhouse, J. H., 2003, Global anisotropic phase velocity maps for fundamental
782 mode surface waves between 40 and 150 s, *Geophys. J. Int.,* 154, 154-165.

783 Vauchez, A., Nicolas, A., 1991, Mountain building: strike parallel motion and mantle anisotropy,
784 *Tectonophysics,* 185, 183-201.

785 Vinnik, L. P., Farra, V., Romanniwicz, B., 1989, Azimuthal anisotropy in the earth from
786 observations of SKS at GEOSCOPE and NARS broadband stations, *Bull. Seis. Soc. Am.,*
787 79(5), 1542-1558.

788 Vinnik, L. P., Green, R. W. E., Nicolaysen, L. O., 1996, Seismic constraints on dynamics of the

789 mantle of the Kaapvaal craton, *Phys. Earth Planet. Int.*, 95, 139-151.

790 Vinnik, L. P., Kosarev, G. L., Makeyeva, L. I., 1984, Anisotropiya litosfery po nablyudeniyam
791 voln SKS and SKKS, *Dokl. Akad. Nauk USSR* , 278, 1335-1339.

792 Waite, G. P., Schutt, D. L., Smith, R. B., 2005, Models of lithosphere and asthenosphere
793 anisotropic structure of the Yellowstone hot spot from shear wave splitting, *J. Geophys.*
794 *Res.*, 110, B11304, doi:10.1029/2004JB003501

795 Walker, K. T., Bokelmann, G. H. R., Klemperer, S. L., 2001, Shear-wave splitting to test mantle
796 deformation models around Hawaii, *Geophys. Res. Lett.,* 28, 4319-4322.

797 Walker, K. T., Bokelmann, G.H.R., Klemperer, S.L., 2004, Shear-wave splitting beneath the
798 Snake River Plain suggests a mantle upwelling beneath eastern Nevada, USA, *Earth.*
799 *Planet. Sci. Let.*, 222, 529-542.

800 Walker, K. T., Bokelmann, G. H. R., Klemperer, S. L., Bock, G., 2005, Shear-wave splitting
801 around the Eifel hotspot: evidence for a mantle upwelling, *Geophys. J. Int.,* 163(3), 962-
802 980.

803 Walker, K. T., Nyblade, A. A., Klemperer, S. L., Bokelmann, G. H. R., Owens, T. J., 2004, On the
804 relationship between extension and anisotropy: Constraints from shear wave splitting
805 across the East African Plateau, *J. Geophys. Res.,* 109(B18), B08302.

806 Watson, G. S., 1985, Interpolation and smoothing of directed and undirected line data, *in* P. R.
807 Krishnajah, ed., Multivariate Analysis-VI, Elsevier Science, New York, , pp. 613-625.

808 Wehrle, V., 1998, Analytische Untersuchung intralithosphärischer Deformationen und Numerische
809 Methoden zur Bestimmung krustaler Spannungsdomänen, PhD thesis (in german), Univ.
810 Karlsruhe, http://digbib.ubka.uni-karlsruhe.de/volltexte/12098

811 Wolfe, C. J., Silver, P. G., 1998, Seismic anisotropy of oceanic upper mantle: Shear wave splitting
812 methodologies and observations, *J. Geophys. Res.,* 103(B1), 749-771.

813 Wolfe, C. J., Solomon, S. C., Shear-Wave Splitting and Implications for Mantle Flow Beneath the
814 MELT Region of the East Pacific Rise, *Science*, 280, 1230-1232, doi:
815 10.1126/science.280.5367.1230

816 Wüstefeld, A., Bokelmann, G. H. R, 2007, Null Detection in Shear-Wave Splitting Measurements,
817 *Bull. Seism. Soc. Am.,* 97(4), 1204-1211, doi:10.1785/0120060190.

818 Wüstefeld, A., Bokelmann, G. H. R., Barruol, G., 2009, Lithospheric anisotropy and deformation
819 beneath the East European Craton, *Tectonophysics,* in press,
820 doi:1010.1016/j.tecto.2009.01.010

821 Xue, M., Allen, R. M., 2007, The Fate of the Juan de Fuca Plate: Implications for a Yellowstone
822 Plume Head, *Earth Planet. Sci. Lett.,* 264, 266-276, doi:10.1016/j.epsl.2007.09.047

823 Zandt, G. and Humphreys, E., 2008, Toroidal mantle flow through the western U.S. slab window,
824 *Geology*, 36(4), 295-298, doi:10.1130/G24611A.1

825

826 **Figure Captions**

827 Figure 1: Paths and spatial resolution associated with teleseismic (SKS) shear waves and surface
828 waves. Surface waves propagate along the surface of the Earth, while wave paths of
829 teleseismic shear waves are nearly vertical. For the latter, there is a progressive time delay
830 between the two (split) shear-waves on the path toward the station at the Earth's surface.

831

832 Figure 2: Global comparison of shear-wave splitting parameters: a) measured b) predicted. a)
833 World-wide shear-wave splitting observations contained in the splitting database. b):
834 predicted splitting values calculated using the method of Montagner et al. (2000) for the
835 1°x1° anisotropic tomography model of Debayle et al. (2005) at depths between 50 and
836 500km. Values are displayed on a 3°x3° grid. The regions which are analysed in further
837 detail in the text are marked (a-h)

838

839 Figure 3: Statistical distribution of 2286 globally distributed shear-wave splitting measurements
840 contained in the current SKS splitting database. a) shows the distribution of delay times, b)
841 that of fast split directions. The statistical distributions of predicted splitting parameters,
842 calculated from surface wave anisotropy (Debayle et al., 2005) are presented separately
843 for continents (c, d) and oceans (e, f). See text for discussion.

844

845 Figure 4: Coherence of the SKS splitting parameters with the predicted splitting values integrating
846 anisotropy between 50 to 500 km depth, for "correlation lengths" D_{corr} of 5, 10, and 20
847 degrees. Several combinations of datasets are tested, such as the effect of a 1° and 10° grid
848 of predicted values and a limited set of data (e and f): studies published before 1997,
849 corresponding to dataset of Silver (1996)). See text for discussion.

Figure 5: Smoothed version of shear-wave splitting observations. Smoothing parameters are chosen as R = 600 km and $\lambda = 5$ (cf. Figure 7). Calculation was for a 1°x1° grid, displayed on a 3°x 3° grid

Figure 6: a) Coherence function using the smoothed splitting data of Figure 5. Three different values for R are used (100, 600, 1000 km), as well as a smoothing value $\lambda = 5$. b) Coherence value as a function of search smoothing parameter λ at 0° misfit. c) and d) show the same as a) and b) respectively, but for a randmised distribution of splitting parameters to test for inherent correlation of the two models. Note the much lower amplitude of correlation in c) and the random variation in d).

Figure 7: Correlation of the smoothed splitting parameters (similar to Figure 4), for individual regions shown in Figure 5.

Figure 8: Map of the predicted (blue), observed (red, with circle marker) and smoothed (magenta with small arrow head) shear wave splitting data in a) Western US and b) Kaapvaal Craton where the tomographic model (i.e., predicted splitting) seems to be dominated by the African Super Swell. Differences in coherence magnitude (Figure 7) are caused by different delay time due to damping effects in the tomography.

Figure 9: Scatter-plot of predicted splitting delay versus observed splitting delay. The predicted delay times are generally smaller, indicating a bias from the tomography, probably due to

873 damping effects.

874

875 Figure A1: Map of the predicted (blue), observed (red, with circle marker) and smoothed (magenta
876 with small arrow head) shear wave splitting data in the Andes.

877 Figure A2: Map of the predicted (blue), observed (red, with circle marker) and smoothed (magenta
878 with small arrow head) shear wave splitting data in the East Pacific.

879 Figure A3: Map of the predicted (blue), observed (red, with circle marker) and smoothed (magenta
880 with small arrow head) shear wave splitting data in the North America.

881 Figure A4: Map of the predicted (blue), observed (red, with circle marker) and smoothed (magenta
882 with small arrow head) shear wave splitting data in East Africa.

883 Figure A5: Map of the predicted (blue), observed (red, with circle marker) and smoothed (magenta
884 with small arrow head) shear wave splitting data in Central Asia.

885 Figure A6: Map of the predicted (blue), observed (red, with circle marker) and smoothed (magenta
886 with small arrow head) shear wave splitting data in Australia

Figure1

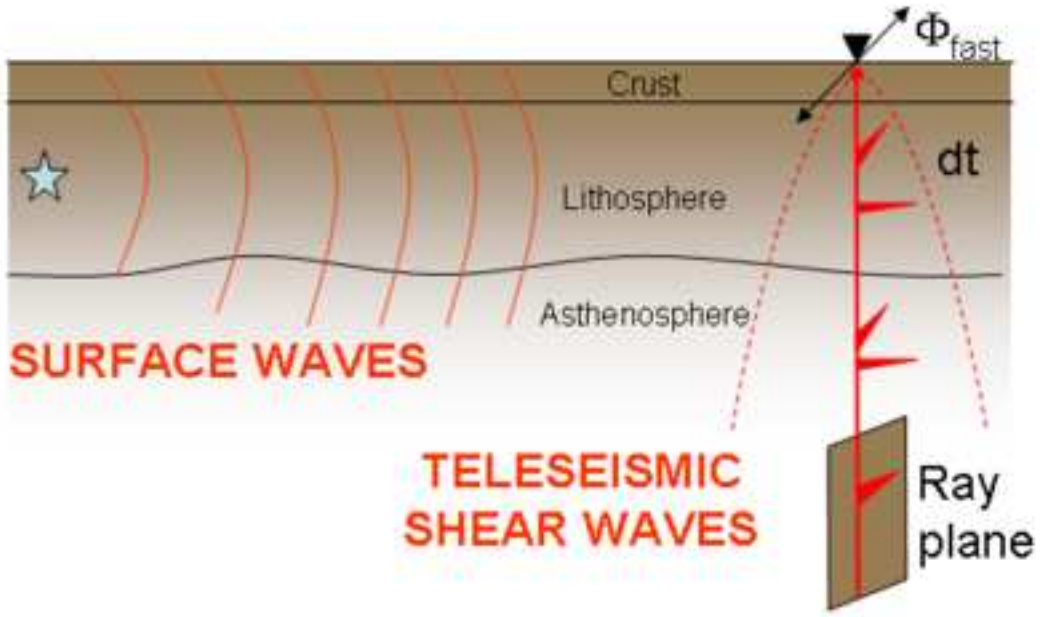
Φfast
Crust
dt
Lithosphere
Asthenosphere
SURFACE WAVES
TELESEISMIC
SHEAR WAVES
Ray
plane

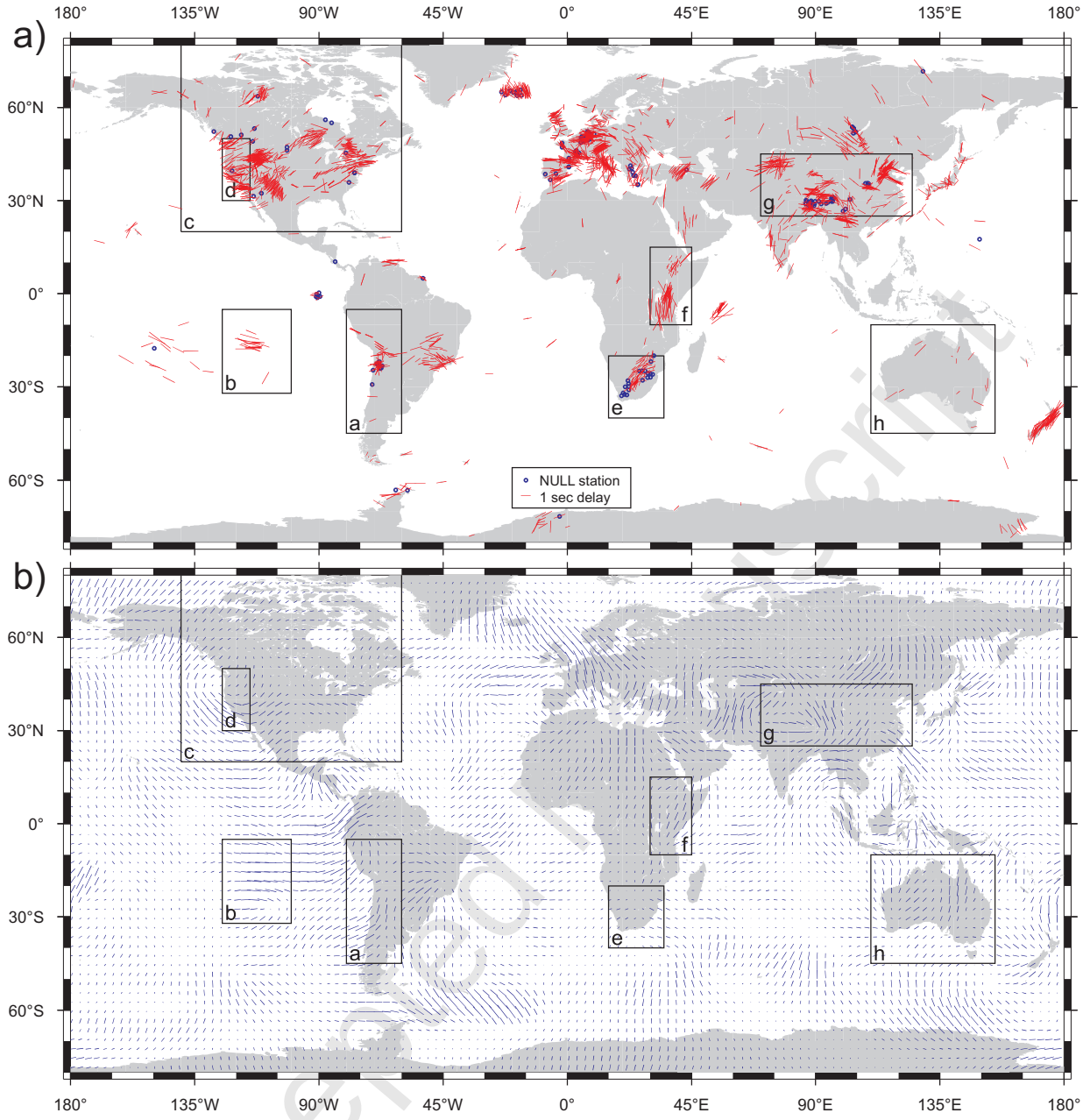

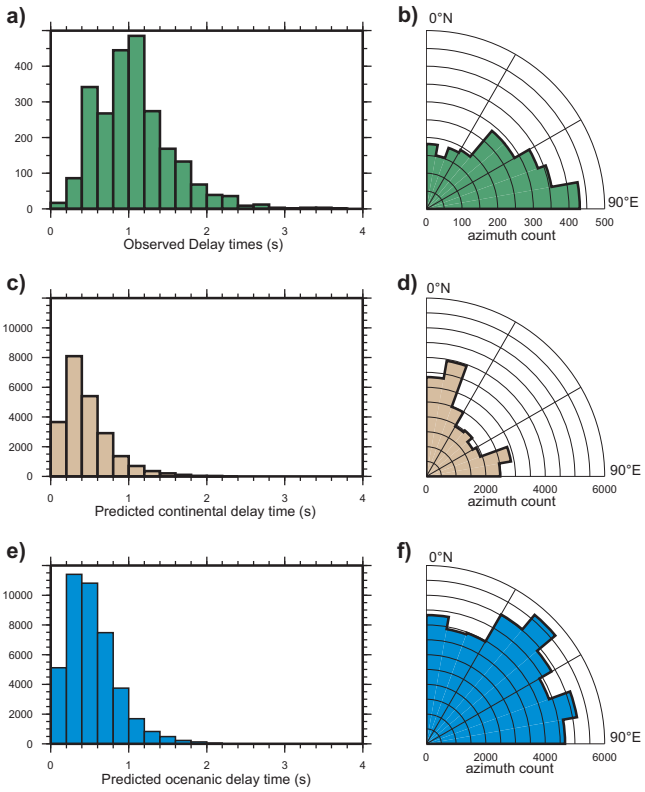

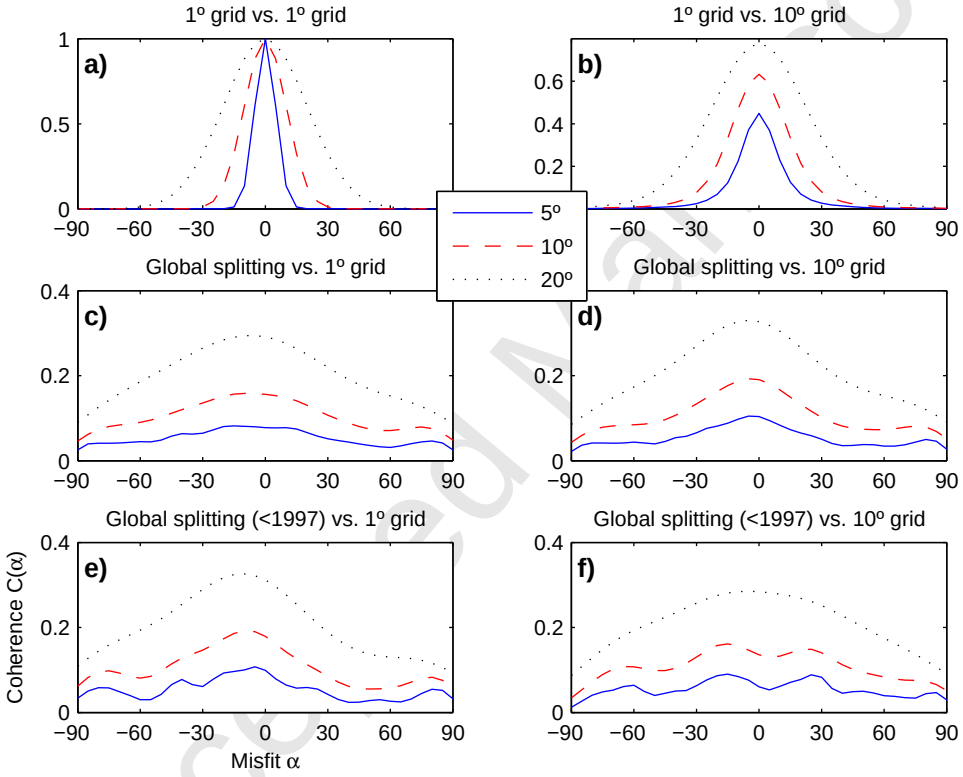

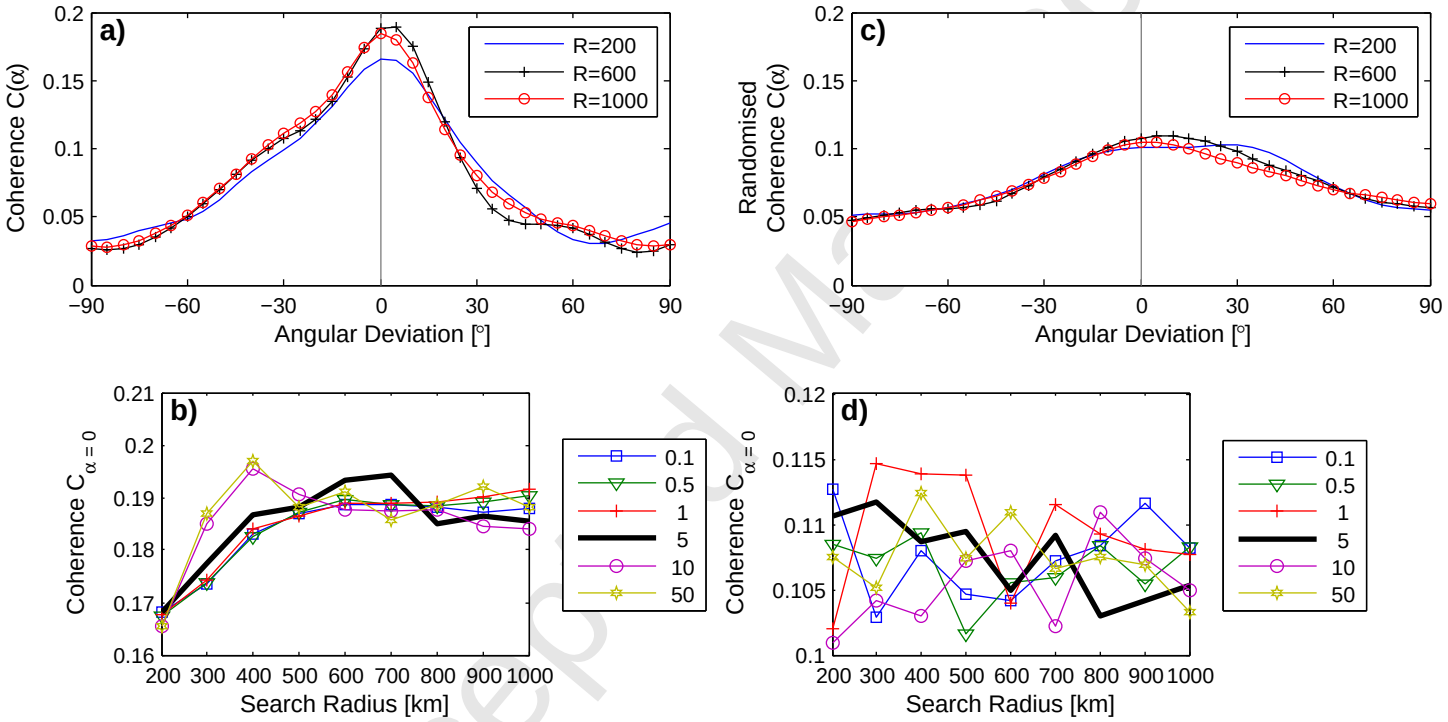

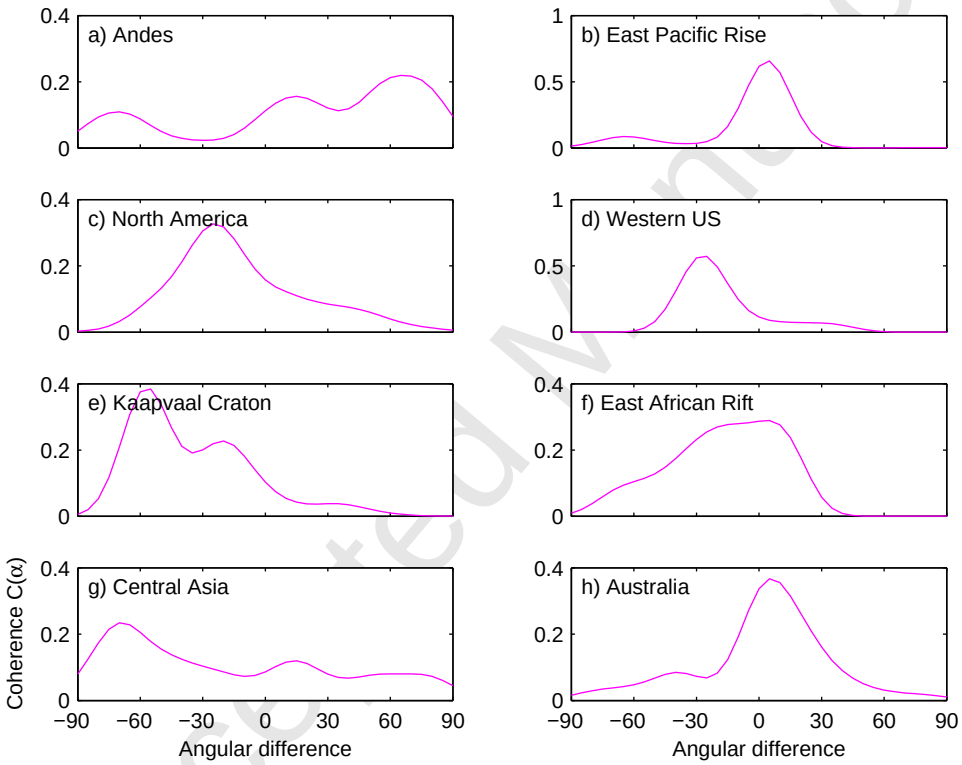

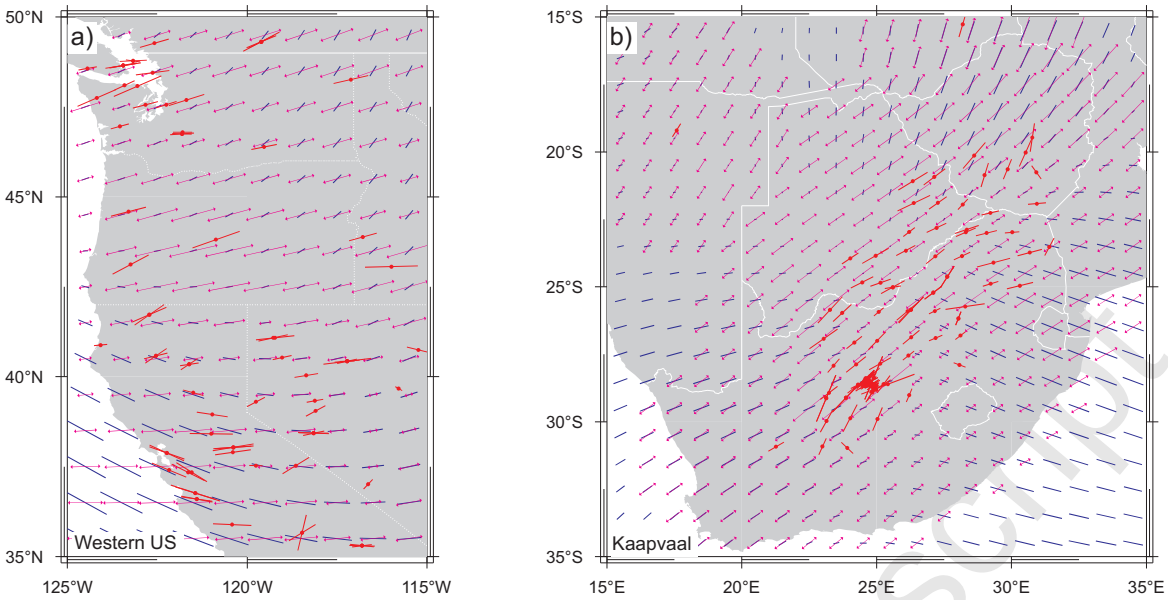

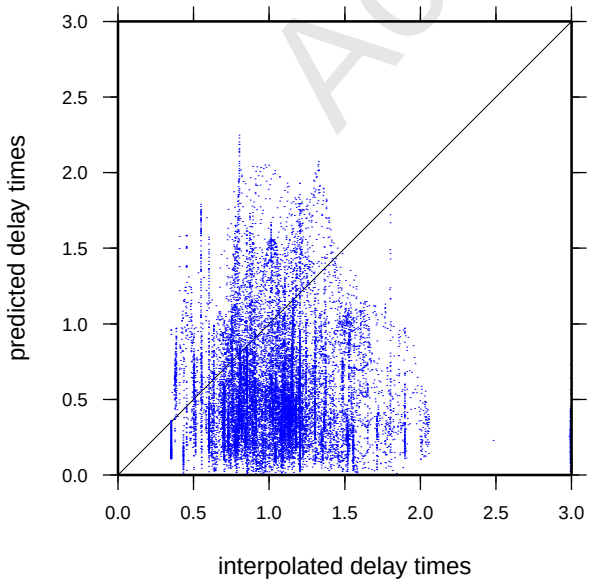

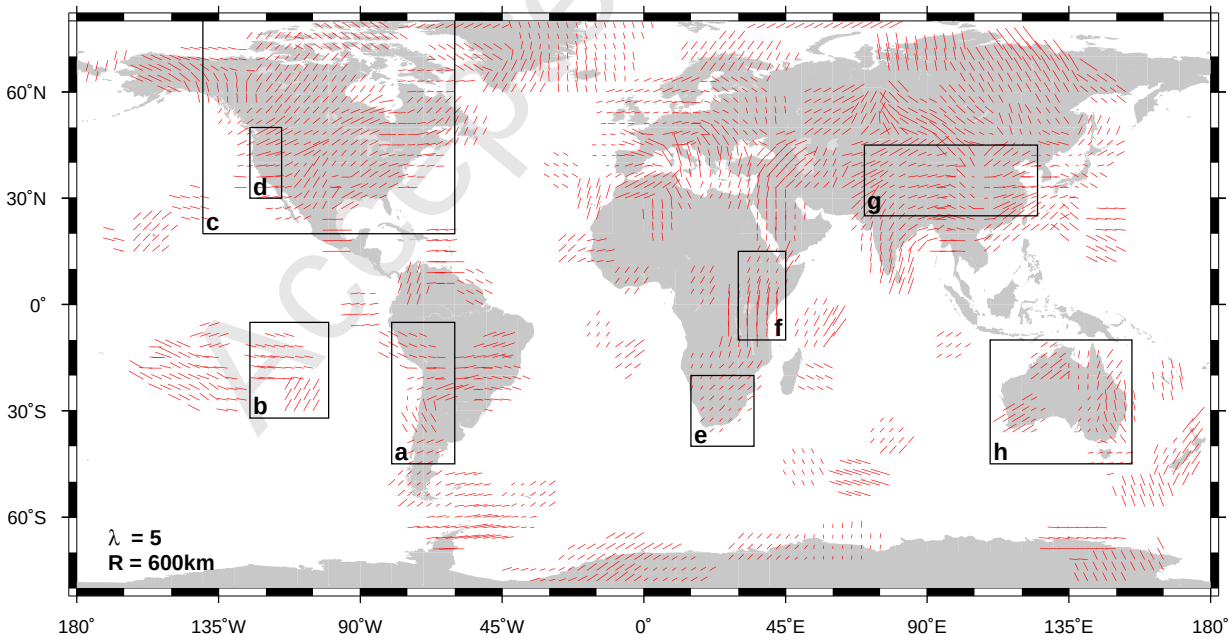

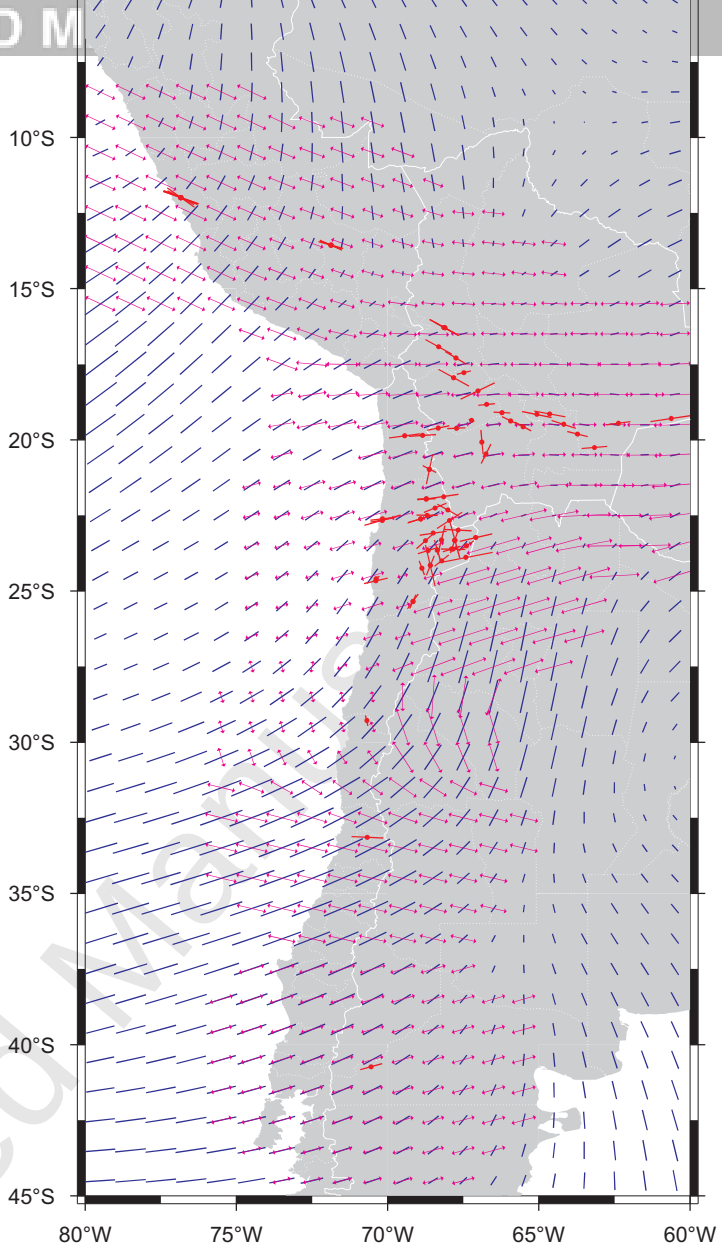

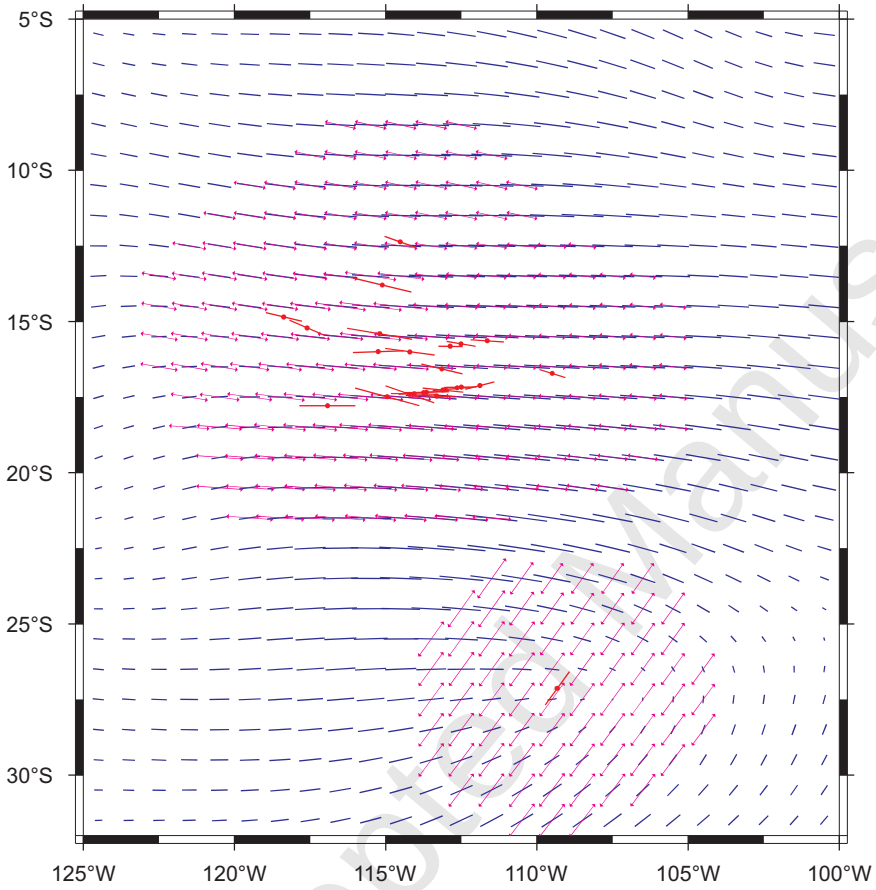

Apendix Figure A3